

AN IONIZED ACCRETION DISK IN CYGNUS X-1

C. DONE,^{1,2} J. S. MULCHAEY,^{3,4} R. F. MUSHOTZKY, AND K. A. ARNAUD³

Laboratory for High Energy Astrophysics, NASA/Goddard Space Flight Center, Greenbelt, MD 20771

Received 1991 September 30; accepted 1992 February 19

ABSTRACT

We have analyzed archival *EXOSAT* and *HEAO 1-A2* observations of Cyg X-1. We find, in agreement with Ebisawa, that the X-ray spectrum of Cyg X-1 exhibits a “high-energy excess” above 8 keV, similar to that seen in *Ginga* spectra of active galactic nuclei. We show for the first time, using a likelihood ratio test, that the data are significantly better fit by a Compton reflection model than by a partial covering model. Even with the energy resolution of the *EXOSAT* GSPC we find that the derived iron line energy and shape are very dependent on the continuum model used. Using the best-fit Compton reflection model we find that the Fe line is not required to be either redshifted or broadened, although the data cannot distinguish between the skewed line profile expected from an illuminated accretion disk and a Gaussian line shape.

The extended, 2–60 keV, energy response of the *HEAO 1-A2* data can constrain the intrinsic continuum form. We find that the best-fit temperature for a Sunyaev-Titarchuk Comptonization model is significantly larger than that found in previous analysis based primarily on data in the 30–150 keV band. This suggests that the 5–50 keV continuum is not well fit by the same spectral form applicable at high energies and that a multiple temperature thermal Compton model is necessary to fit the broad-band data.

The relative intensity of the Compton reflection component, combined with the known parameters of the Cyg X-1 system, is consistent with several models of the system, namely:

1. A point source origin of the X-ray emission situated above a flat disk with twice cosmic abundances, or
2. A spherical, optically thick source at the center of flat disk in which only Fe is over abundant, or
3. A optically thick source at the center of a flared disk with twice solar abundance.

The measured Fe edge in the reflection spectrum is predominantly due to iron more ionized than Fe xv, inconsistent with that expected from a Shakura-Sunyaev disk. However the relatively low equivalent width of the Fe line, 44 ± 28 eV is considerably smaller than that expected from a disk also responsible for the high-energy continuum. Only the line predicted from (3) gives a line within $\sim 3 \sigma$ of that observed, but a similar effect seen in other X-ray binary systems suggests that the lack of direct connection between the line intensity and reflection spectrum normalization may be a more widespread problem in models of X-ray illuminated accretion disks.

Subject headings: accretion, accretion disks — radiation mechanisms: Compton and inverse Compton — stars: individual (Cyg X-1) — X-rays: stars

1. INTRODUCTION

Cyg X-1 is a well-known Galactic black-hole candidate (McClintock 1986), in a 5.6 day binary orbit around the O9.7 Iab star HD 226868 (Gies & Bolton 1986). The intense X-ray emission from the compact object is thought to be powered by accretion of matter from the companion star and a further period of 294 days (Priedhorsky, Terrel, & Holt 1983), seen in both optical and X-ray data, is thought to be associated with precession of the accretion disk. This putative Galactic black-hole/accretion disk system exhibits many similarities in its X-ray emission characteristics to the supermassive black-hole/accretion disk systems that are thought to comprise the energy generation mechanism of active galactic nuclei (AGNs) (see White, Fabian, & Mushotzky 1984).

Cyg X-1 has a highly variable hard X-ray spectrum, which can be characterized as a power law between 2–10 keV of index $\alpha \sim 0.5$ –0.9 (see e.g., the review by Liang & Nolan 1984), showing iron $K\alpha$ line emission at around 6 keV (Barr, White, &

Page 1985). Below 3 keV there is a contribution from a softer flux spectrum, thought to be thermal emission from an accretion disk (Balucinska & Hasinger 1992), and also a line at 700 eV, probably from complex iron L shell emission (Barr & Van der Woord 1990). All of these characteristics can be found in AGN X-ray spectra, with suitable scaling for the mass of the central object giving the longer variability time scales and lower energy of the accretion disk spectrum in AGNs (Mushotzky 1982; Turner & Pounds 1989; Awaki 1990; Pounds 1992; Turner et al. 1992). Hence an understanding of the X-ray emission spectrum of Cyg X-1, may also be applicable to AGNs and vice versa.

Recent data on AGN from the *Ginga* satellite have indicated systematic deviations from a simple power-law spectrum in the 2–20 keV band (Pounds et al. 1989; Nandra et al. 1989; Piro, Yamauchi, & Matsuoka 1990; Pounds et al. 1990; Matsuoka et al. 1990). The aforementioned Fe $K\alpha$ line is often seen, together with a decrement between 7–9 keV and an excess of counts above 10 keV, the so-called “high-energy excess.” These features are consistent with the idea that the X-rays are reprocessed by material which subtends a substantial solid angle to the X-ray source. A self-consistent interpretation of these features is that the X-rays are reflected and reprocessed in an optically thick accretion disk (Lightman & White 1988; Guil-

¹ NRC-GSFC Research Associate.

² Postal Address: Department of Physics and Astronomy, University Road, University of Leicester, Leicester, LE1 7RH, UK.

³ Also Astronomy Program, University of Maryland.

⁴ Also Space Telescope Science Institute.

bert & Rees 1988). The reflection albedo is energy dependant, as at low energies the reflection probability is decreased by photoelectric absorption, whereas at higher energies Compton downscattering and the reduction of the scattering cross section deplete the number of photons reflected. This results in a broad-band spectral “bump,” centered around 20 keV, but the dependance on photoelectric absorption at low energies gives a pronounced feature at the iron K edge energy in the reflected spectrum and an associated Fe K α fluorescence line, which has a characteristic skewed profile due to doppler and gravitational effects (Fabian et al. 1989).

If Cyg X-1 does contain an accretion disk, then this reflection signature should also be present in its X-ray emission. In fact, the characteristic pattern of residuals can be seen in published data (Fabian et al. 1989; cf., Pounds et al. 1990), and the edge feature has been noted by Balucinska & Barr (1992). However, while reflection gives a physically compelling explanation of these features, an alternative description of the spectra is a partially covered power-law source, where the covering column is large, $N_{\text{H}} \sim 10^{24} \text{ cm}^{-2}$ (Piro et al. 1990; Matsuoka et al. 1990). This gives the observed edge and excess of counts above 10 keV, but the spectral shape is subtly different from that of reflection. At low energies the partially covered spectrum is more strongly depressed as all the covered flux goes through the same absorbing column whereas reflection occurs at a range of absorbing depths in the material. Conversely, at high energies the partially covered flux is larger than that from reflection as it is unaffected by the Compton downscattering inherent in the reflection process. Thus, in principle, the two models can be distinguished, but the poor signal-to-noise of AGN data do not allow this test.

In this paper we use high signal-to-noise archival *EXOSAT* and *HEAO 1-A2* data on Cyg X-1 to determine whether there is a counterpart in the Cyg X-1 spectra of the “high-energy excess” seen in AGNs, and whether this is best fitted by reflection or partial covering. This is the best test to date of reflection models, as the *HEAO 1* data extend out to 50 keV, allowing the best determination of the shape of the “high-energy excess,” and the energy resolution of the *EXOSAT* GSPC enables an accurate measure of the energy of the iron edge. A preliminary, independent observation of the “high-energy excess” in *Ginga* data on Cyg X-1 and other X-ray binary sources and its interpretation in terms of reflection can be found in Tanaka (1992), Ebisawa (1991), and Mitsuda (1992).

We find that the data are considerably more likely to be described by Compton reflection rather than partial covering, though we are unable to definitively test whether this material corresponds to the accretion disk through the line profile.

While Cyg X-1 can be looked at as a mini-AGN, there is a profound difference between the two systems. The accretion in Cyg X-1 is fueled by a wind from the companion O star, but classic stellar wind accretion is chaotic, forming an unstable accretion wake (see, e.g., Kallman, Stevens, & Blondin 1992) rather than a disk. The observation that Cyg X-1 has a stable, long-lived accretion disk favors the “focused wind accretion” theories (Friend & Castor 1982), in which the disk is stabilized by the massive star being extremely close to filling its Roche lobe (Gies & Bolton 1986).

In § 2 we review the relevant X-ray observations of Cyg X-1, followed by a detailed description of the data used for the study in § 3. The reflection spectrum is described in § 4 and used in the model fitting of § 5. Results are discussed in § 6, with a summary in § 7.

2. X-RAY OBSERVATIONS OF THE CYGNUS X-1 SYSTEM

The Galactic absorption in the direction of Cyg X-1 is characterized by a column of $N_{\text{H}} \sim 7 \times 10^{21}$ (Barr et al. 1985), but the absorption observed is often more than that value during the so-called “dips” (Li & Clark 1974; Mason et al. 1974). The absorption during the dips is generally complex, with more flux at low energies than expected from a cold absorber that completely covered the source (Pravdo et al. 1980). Partial ionization of the absorber was suggested as the reason for the discrepancy, but *Tenma* observations showed that the iron absorption edge energy during the dips was inconsistent with this model (Kitamoto et al. 1984). Hence a more probable explanation is that the very low-energy flux is more extended than the high-energy flux, so is only partially covered by the absorber (Kitamoto et al. 1984). This consistent with the spectral results which suggest a contribution to the soft X-ray spectrum from an extended accretion disk (Balucinska & Hasinger 1991; Barr & Van der Woord 1990), and also by the millisecond time variability of the hard X-ray flux (Miyamoto & Kitamoto 1989), indicating that the hard X-ray source is not extended.

The best estimate of the iron abundance of the system comes from the depth of the iron edge during the dips, giving $A_{\text{Fe}}/A_{\text{H}} = 6 \pm 1 \times 10^{-5}$ (Kitamoto et al. 1984), in contrast to the cosmic abundance of iron of $2.6\text{--}4 \times 10^{-5}$ (Lang 1974; Allen 1973) i.e., that iron is overabundant by a factor ~ 2 relative to cosmic. There are no strong limits on the abundances of any other elements, beyond the fact that the equivalent widths of the UV lines are close to those seen in other OB supergiants (Treves et al. 1980).

The spectrum also shows features associated with absorbing material outside of the dips. A substantial iron K absorption edge with $\tau \sim 0.06$ is sometimes seen in the data, whose strength is not related to the orbital phase (Balucinska & Barr 1992). Similarly, a phase-independent iron line at ~ 6.4 keV of equivalent width $\sim 50\text{--}100$ eV is seen (Barr et al. 1985; Kitamoto et al. 1990). The phase independence of these features suggest that they are associated with the compact object rather than the companion star, and imply that there are large amounts of material close to the X-ray source.

Both iron line and edge are much stronger than expected from the column density measured in the line of sight from the persistent (nondip) low-energy X-ray absorption column (Kallman 1986; Balucinska & Barr 1992). Also, the edge seen in the persistent emission is at 7.5 keV (Balucinska & Barr 1992), considerably higher in energy than the 7.1 keV expected for a cold absorber and higher than the edge at 7.18 ± 0.18 keV seen in the dip spectra (Kitamoto et al. 1984). This suggests that the edge seen in the persistent emission is different in origin from that seen in the dip spectra as the absorbing material is much more strongly ionized.

While the line in the persistent emission is consistent with the 6.4 keV fluorescent line seen from neutral iron (and all ionization states up to Fe XVIII), the line energy derived from fitting the continuum to a power law is systematically redshifted from this energy, so that a weighted mean line energy from all the fits is significantly less than 6.4 keV. The interpretation of this redshift proposed by Barr et al. (1985) and Balucinska & Barr (1992) is that the line is Compton downscattered in a cool accretion disk corona. An alternative scenario is that the line arises from the surface of an X-ray illuminated accretion disk (Fabian et al. 1989), where gravitational redshift and doppler effects can be important.

3. THE DATA

3.1. EXOSAT GSPC and ME

EXOSAT data on Cyg X-1 are available from all three instruments on the satellite, the LE (low energy: 0.5–2 keV), ME (medium energy: 2–20 keV) and GSPC (gas scintillation proportional counter: 2–20 keV). The LE data are sensitive primarily to the low-energy blackbody component so we concentrate on the ME and GSPC spectra, both of which cover the 2–20 keV bandpass. These differ only in that the ME has a higher effective area but with lower spectral resolution than the GSPC. The ME data can extend out to 60 keV in 128 spectral channels, or to 20 keV with 64, 32, or 8 spectral channels.

3.1.1. Data Selection Criteria

The EXOSAT archive data base contains 14 GSPC and 19 on target ME spectra of Cyg X-1. As the 8 channel ME data contains very little spectral information, and the 128 channel ME data is not well calibrated at high energies (N. White 1991, private communication), observations taken in these modes were excluded from the analysis. One further ME spectrum (taken on day 224 of 1985, henceforth 85/224) was excluded as it showed features associated with the “difference spectra” used for background subtraction (Parmar & Izzo 1986). For both the ME and GSPC only data with quality flag 5 (the highest, indicating excellent data) were used, and observations in which dips are seen are discarded (84/206, 85/288), as the complex absorption behavior may dominate over the more subtle spectral effects investigated here. Three further GSPC observations were discarded (85/157, 84/142, 83/268), the first because fluorescence lines at 10.5 and 12.7 keV from lead in the collimator and thorium (decay product of residual plutonium in the detector window) can clearly be seen in the data, indicating that the background subtraction is anomalous in this observation (White 1985), and the latter two because exposure times of <2000 s give poorly constrained parameters in spectral fitting.

A previous analysis of the EXOSAT LE and ME observations of Cyg X-1 by Balucinska & Hasinger (1991) showed that the soft excess makes a significant contribution to the flux even at 2 keV. Also, an instrumental feature from the Xenon detector gas at 4.7 keV can be clearly seen in most of the spectra, so only data above 5 keV are used, to avoid possible contamination.

Although all data below 5 keV are discarded, the spectral fitting is not independent of the column density assumed as the Galactic column is high ($N_{\text{H}} = 7 \times 10^{21} \text{ cm}^{-2}$) and there is evidence for a substantial increase in the absorbing column through the binary period outside of the dip events due to the stellar wind (Kitamoto et al. 1990). Because the subtle effect of variable absorption is convolved with several of the parameters of interest, fitting for absorption enlarges the confidence regions considerably. Hence we have chosen not to include those observations that are not trivially consistent with the Galactic N_{H} .

Details of the selected observations are given in Table 1.

3.2. HEAO 1-A2

The HEAO 1-A2 instrument (Rothschild et al. 1979) observed Cyg X-1 on two separate occasions. Of its six instruments (three high-energy detectors, HED1–3, energy range 2–60 keV; one medium-energy detector, MED1, energy range 2–20 keV; two low-energy detectors, LED1–2, energy range

TABLE 1

OBSERVATION DATES, EXPOSURES AND PHASE INFORMATION
(EPHEMERIS FROM GIES & BOLTON 1986)

Observation	File Number	Detector	Exposure (s)	$\phi_{5.6}$	ϕ_{294}
1977 Nov 17	003	HEAO 1-A2	72060	0.20	0.76
1978 Nov 4	392	HEAO 1-A2	43200	0.06	0.95
1984 Jul 9	08	EXOSAT GSPC	19790	0.25	0.01
1985 Sep 14	09	EXOSAT GSPC	27969	0.40	0.48
1985 Aug 12	10	EXOSAT GSPC	21144	0.45	0.36
1984 Nov 2	13	EXOSAT GSPC	5568	0.99	0.40
1984 Nov 2	14	EXOSAT GSPC	13066	0.12	0.40
1985 Jun 6	01me	EXOSAT ME	14717	0.54	0.14
1984 Jul 9	02me	EXOSAT ME	1357	0.25	0.01
1985 Sep 14	15me	EXOSAT ME	10897	0.42	0.48
1984 Nov 2	17me	EXOSAT ME	4500	0.01	0.41

0.15–4 keV), four were coaligned for source observations and the other two (HED1, LED1) offset for background monitoring. The energy range of the high-energy detectors is best suited for a search for Compton reflection, but as HED2 has a higher background, we use data from HED3 only.

The detectors have both large ($3^\circ \times 3^\circ$) and small ($3^\circ \times 1.5^\circ$) fields of view. Together these give a total effective area around 600 cm², with low associated background due to the effective shielding. However, lack of pointing stability gives an uncertainty in the total exposure time in the small field of view, so the count rate between 10–60 keV was scaled to match that in the large field of view. Comparison of the HED3 Crab data with the expected spectrum of the Crab show that systematic uncertainties are of the order of 0.5%, so the error bars were increased accordingly.

3.2.1. Data Selection Criteria

The HEAO 1-A2 archive contained only two observations of Cyg X-1. All data below 5 keV was discarded as being possibly contaminated by the soft X-ray excess (and Xe L edge). Both data sets have absorption consistent with the Galactic column.

Gain and resolution changes in the detector were tracked with a weak Am²⁴¹ radioactive source, resulting in lines at 59.6, 26.3, 17.8, and 13.9 keV (Robinson-Saba 1983). These were used to calculate a response matrix for the detector at intervals of ~180 days. Both Cyg X-1 observations are midway between such matrix calculations, so extremely weak residuals from all these lines can be seen in the data. To prevent these background features weighting the fit, the data above 50 keV was discarded, as were three channels corresponding to the residuals around each of the features at 13.9, 17.8, and 26.3 keV.

In the first observation, more than half of the data were taken in a high time resolution mode which limited the telemetry rate. The high count rates at low energies were unable to be recorded so data below 10 keV taken in this mode were discarded. Because of the uncertainty in the deadtime corrections, these data were scaled to the 10–50 keV count rate of the data taken in the normal, higher telemetry mode. Details of the observations are given in Table 1.

4. THE REFLECTION MODEL

We are interested in whether the signature of a Compton reflection spectrum is seen, and so have to model the effects of reflection. In general this is a complex procedure as the spectral shape depends on:

1. the geometry of the material (George & Fabian 1991; Matt, Perola, & Piro 1991);
2. the ionization state of the material (Lightman & White 1988);
3. the elemental abundances (George & Fabian 1991; Matt et al. 1991);
4. the orientation of the system to the observer (George & Fabian 1991; Matt et al. 1991); and
5. the geometry of the X-ray source (George & Fabian 1991; Matt et al. 1991).

The detailed modeling of these is dealt with in the Appendices. Note that this is only the modeling of the continuum and does not include spectral line features which are treated separately.

Here we restrict discussion to the underlying physical principles to give some intuitive feel of how reflection varies with these parameters. The general shape of the reflection spectrum has already been described in the Introduction, as a broad peak between 10–100 keV with reflection at low energies being suppressed by photoelectric absorption and at high energies by the combined effects of Compton downscattering, the decrease in the scattering cross-section and the predominance of forward rather than back scattering (see Lightman & White 1988 for a more detailed discussion of the standard reflection spectral shape).

The dependence of the amount of reflection on the geometry of the reflecting material is simply that the larger the solid angle of material available for reflection the larger the contribution of the reflected component to the total (direct plus reflected) spectrum. This affects the reflected spectrum at all energies.

The dependence on ionization, abundance and inclination can also be easily understood. In order to see reflection, the illuminating photons must be Compton scattered into the observers line of sight and must then escape without being photoelectrically absorbed by the intervening material. Ionization reduces the low-energy opacity of the material, reducing the chance of absorption and so increasing the amount of reflection seen at low energies. Similarly, increasing the elemental abundances increases the opacity and hence decreases the probability of reflection. The inclination of the material to the line of sight determines the path length of the scattered photons through the material. The higher the inclination, the longer the path, leading to a higher optical depth transversed by the scattered photons and hence a smaller reflected contribution. These mainly affect only the part of the reflection spec-

trum below 20 keV, where photoelectric absorption is the dominant effect.

The effect on the reflection spectrum of the source shape is a little more subtle. It depends in part on the average incident angle of the illuminating photons. If the photons enter the surface at a grazing angle, then they reach a Thomson depth of unity (the average place for Compton scattering) along their path length whilst only at a small vertical distance from the surface. Thus the escape probability is larger than if the incident angle was close to normal to the surface of the material, where a Thomson depth of unity along the incident path takes the photon much deeper into the material. Thus a point source above the disk gives more reflection than an extended, optically thin corona covering most of the disk (around 50% more below 20 keV). However, there is a further complication, and that is if the source is optically thick, where the source itself can shield the material from the illuminating X-rays, so reducing the apparent solid angle of material and so reducing the reflected component. A central, optically thick source only provides half as much reflection as produced by a point source (see Chen & Halpern 1989; Matt et al. 1991).

5. MODEL FITS

For the *HEAO 1* and ME data, no detailed information can be obtained on the line energy or width because of the relatively low ($E/\Delta E \sim 6$) spectral resolution of the detectors. These parameters are thus fixed at 6.4 and 0.3 keV, respectively. However, the better spectral resolution of the *EXOSAT* GSPC detector ($E/\Delta E \sim 12$) allows the line energy and width to be determined from the fits. The absorption is fixed at the Galactic value of $7 \times 10^{21} \text{ cm}^{-2}$ (see § 3.1.1 for discussion of this point) in all the fits described below.

We show in Figure 1 the residuals of a simple galactic absorption and power-law fit to one of the *EXOSAT* GSPC and one of the *HEAO 1*-A2 observations. Notice that both data sets show strong positive residuals around 6.4 keV, negative residuals between 8–12 keV, and positive residuals above 12 keV indicative of a spectral flattening. These features (an Fe $K\alpha$ line, a pseudo-edge and reflection hump) are exactly those predicted in Compton reflection models (George & Fabian 1991).

5.1. Power Law, Line and Edge

Fits of a model comprising of galactic absorption, power-law, line, and edge are shown in Table 2. The curvature present in the spectrum (high-energy flattening) distorts the fit,

TABLE 2
FITS TO A MODEL OF GALACTIC ABSORPTION, POWER LAW, GAUSSIAN LINE, AND EDGE

File Number	$\Gamma = \alpha + 1$	N_a	E_{line} (keV)	σ_{line} (keV)	$10^{-3} N_{\text{line}}$	EW (eV)	E_{edge} (keV)	$10^{-2} \tau_{\text{edge}}$	χ^2/pha
08	1.61 (1.60, 1.63)	1.20 (1.16, 1.27)	5.88 (5.77, 6.05)	1.0 (0.80, 1.0)	21 (14, 24)	290 (211, 335)	9.2 (7.1, 9.2)	1 (0, 2)	102/140
09	1.43 (1.41, 1.45)	0.95 (0.90, 1.02)	5.81 (5.67, 6.06)	1.0 (0.89, 1.0)	22 (16, 27)	284 (207, 339)	7.2 (7.1, 8.83)	1 (0, 5)	119/106
10	1.54 (1.53, 1.55)	1.10 (1.06, 1.12)	6.50 (6.32, 6.59)	0 (0, 0.38)	2.56 (1.87, 3.94)	41 (30, 64)	7.74 (7.53, 7.98)	5 (3, 6)	99.1/115
13	1.68 (1.63, 1.70)	2.21 (1.90, 2.30)	6.34 (5.78, 6.52)	0.27 (0, 1.0)	3.87 (1.79, 2.36)	39 (17, 214)	7.70 (7.35, 7.84)	8 (4, 10)	169/169
14	1.59 (1.57, 1.62)	1.43 (1.34, 1.54)	5.72 (5.54, 5.94)	1.0 (0.87, 1.0)	18 (10, 26)	192 (114, 279)	7.70 (7.49, 7.99)	4 (3, 7)	94.5/113
01me	1.55 (1.52, 1.57)	1.07 (0.99, 1.13)	6.4	0.3	1.51 (0, 4.30)	25 (0, 73)	7.92 (7.68, 8.20)	11 (8, 14)	32.1/41
02me	1.67 (1.63, 1.71)	1.41 (1.30, 1.53)	6.4	0.3	1.12 (0, 4.50)	18 (0, 71)	8.07 (7.46, 8.50)	13 (6, 19)	11.3/21
15me	1.54 (1.53, 1.56)	1.37 (1.32, 1.41)	6.4	0.3	0 (0, 1.73)	0 (0, 22)	8.13 (7.83, 8.33)	13 (10, 15)	30.8/43
17me	1.64 (1.63, 1.67)	1.97 (1.93, 2.08)	6.4	0.3	1.36 (0, 2.71)	2 (0, 29)	8.20 (7.97, 8.41)	12 (9, 15)	26.5/43
o003	1.45 (1.44, 1.46)	1.16 (1.13, 1.19)	6.4	0.3	1.01 (0, 3.25)	13 (0, 42)	8.12 (7.97, 8.27)	14 (12, 16)	112/112
o392	1.45 (1.45, 1.47)	1.03 (1.02, 1.04)	6.4	0.3	0 (0, 0.53)	0 (0, 8)	8.03 (7.91, 8.14)	13 (11, 14)	148/66

NOTES.—The line width is constrained to be less than 1 keV in fits to the GSPC. The normalizations N_a and N_{line} have units of photons $\text{cm}^{-2} \text{ s}^{-1} \text{ keV}^{-1}$ and all errors are 90% confidence limits.

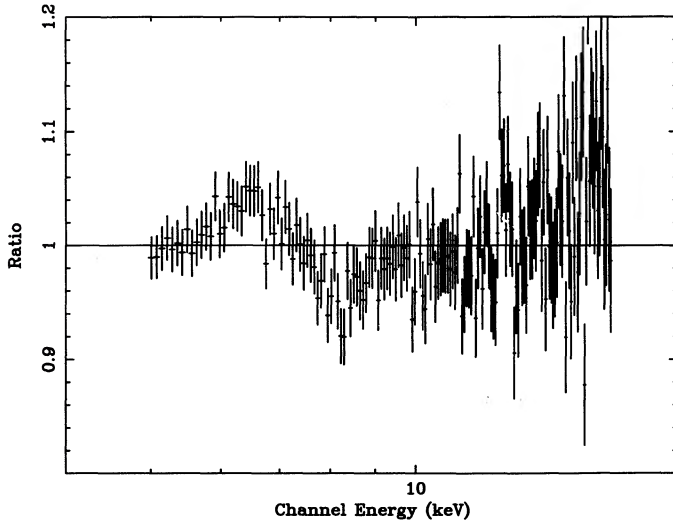


FIG. 1a

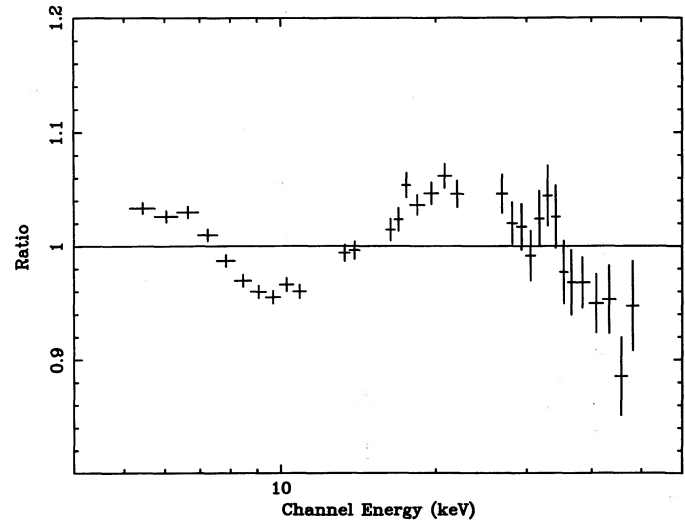


FIG. 1b

FIG. 1.—(a) Ratio of residuals (data/model) from one of the GSPC spectra (13) to a model of galactic absorption and a simple power law. The model is a poor fit to the data, with the residual being systematically high at ~ 6 keV, low at 7–9 keV, rising again towards higher energies. (b) Same pattern present in one of the *HEAO 1-A2* spectra (o392).

resulting in an artificially large, broad, redshifted line which reproduces the steeper low-energy spectrum rather than the line itself. In order to constrain the line to be a sharp rather than a “continuum” feature, the line width was required to be less than 1 keV in the fits to the GSPC data. This limit is more than the line widths predicted by the two models of line broadening previously suggested, namely Comptonization and gravitational/Doppler effects, so it should not restrict any physically meaningful fits. Balucinska & Barr (1992), who also fitted this model, included the flux down to 3 keV. This constrains the worst of these unphysical effects.

The model generally gives an acceptable fit to the data, with $\chi^2_\nu/\nu \leq 1.5$. The addition of an edge gives a significantly better fit (90% error bars on the depth of the edge not including zero) in all but two of the spectra. Where the edge is significant, it is always at substantially higher energies than expected for cold material, with 90% confidence limits indicating a range from 7.35–8.50 keV, i.e., Fe x–xxiii, consistent with that found by Balucinska & Barr (1992). This range predicts that the iron line energy should be 6.4–6.6 keV. Where the line energy can be determined (GSPC data), it is inconsistent with this value in three of the five cases. The spectra that do not fit this physical constraint have a best-fit line that is extremely broad, redshifted, and has a large equivalent width of ~ 250 eV, where the broad-line feature mimics a steeper low-energy continuum, as discussed above.

5.2. Partially Covered Power-Law Continuum and Line

This is a substantially better fit to the data than a simple edge, as it gives a means of flattening the high-energy spectrum. Note that the line energy is now around 6.4 keV in all but one of the GSPC spectra, and also that the edge is now produced from cold material, i.e., at 7.1 keV. This illustrates the general uncertainty that affects modeling of X-ray spectral features, and we note that the sense of the change in the line (redshift and broadening) is the same as expected for the physical effects of Comptonization and disk angular momentum effects. Unless the continuum is modeled correctly the derived parameters of any spectral features are not meaningful (cf., the discussion of this point in Kitamoto et al. 1984), even in a detector

of moderate spectral resolution. Table 3 gives the best-fit parameters while Figures 2a and 2b show typical GSPC residuals and model spectra, respectively.

Note that this model, although a better fit to the data, is not physically correct. The very large column densities inferred require that Thompson scattering be considered as an important modification to the partially covered spectrum (see Makashima 1986, and references therein). As this is not included in the spectral fitting model, the results are not completely self-consistent. This caveat applies also to the AGN results for partial covering discussed by Piro et al. (1990) and Matsuoka et al. (1990).

5.3. Power Law, Line, and Reflection Spectrum

We fit each spectrum in turn with a model of a power law, Compton reflector and Gaussian line. The disk temperature is fixed at 10^5 K, as appropriate for the surface temperature of a disk around a $\sim 10 M_\odot$ compact object. The disk inclination is fixed at 30° (Gies & Bolton 1986) and we assume that the X-ray source emits isotropically. The derived model parameters are given in Table 4 and typical GSPC residuals and model spectra are shown in Figures 3a and 3b, respectively.

The best-fit reflection spectrum is always indicative of ionized material, with neutral material excluded at the 90% confidence level in all of the *HEAO 1* spectra, three of the four ME spectra and three of the five GSPC spectra. The level of ionization, is defined by the ionization parameter $\xi = L/nr^2 = 43 \pm 25$ (see Fig. 5), where ξ is the ionization parameter, L is the integrated incident luminosity between 5 eV and 300 keV, n is the density of the material and r is the distance of the material from the illuminating source. This value of the ionization parameter corresponds to Fe xv (with an edge at 7.6 keV for an illuminating power law with $\alpha = 0.7$).

This is generally the best fitting model. There are no remaining significant residuals and χ^2_ν/ν is close to unity. While partial covering also gave an acceptable fit, reflection gives a smaller χ^2_ν/ν in 9 of the 11 spectra. The ratio of likelihoods $L_1/L_2 = e^{(\chi^2_2 - \chi^2_1)/2}$ can be used to quantify the difference in goodness of fit (Edwards 1972; Mushotzky 1982; Barr & Van der Woord

TABLE 3
 FITS TO A MODEL OF GALACTIC ABSORPTION, POWER LAW, GAUSSIAN LINE, AND PARTIAL COVERING

File Number	$\Gamma = \alpha + 1$	N_g	E_{line} (keV)	σ_{line} (keV)	$10^{-3}N_{\text{line}}$	EW (eV)	$10^{22}N_{\text{H}}$ cm $^{-2}$	$10^{-2}f_{\text{cov}}$	χ^2_{ν}/pha
08	1.70 (1.64, 1.75)	1.66 (1.35, 1.94)	6.22 (5.96, 6.44)	0.71 (0.50, 0.97)	11 (7.0, 19)	146 (92, 258)	396 (250, 740)	11 (5, 16)	96.4/140
09	1.53 (1.46, 1.61)	1.41 (1.15, 1.78)	6.19 (5.82, 6.58)	0.62 (0, 0.95)	10 (3.5, 22)	119 (40, 241)	544 (330, 1450)	16 (10, 23)	101/106
10	1.61 (1.58, 1.63)	4.63 (2.40, 6.75)	6.52 (6.41, 6.61)	0.33 (0.08, 0.52)	16 (11, 22)	70 (51, 79)	5390 (3020, 25500)	74 (58, 82)	86.4/115
13	1.77 (1.69, 1.83)	3.07 (2.47, 3.61)	6.38 (6.06, 6.57)	0.56 (0.35, 0.87)	11 (7.3, 21)	97 (63, 181)	239 (138, 550)	18 (11, 24)	170/169
14	1.60 (1.58, 1.64)	1.73 (1.66, 3.41)	5.70 (5.58, 5.90)	1.0 (0.86, 1.0)	28 (19, 34)	249 (180, 300)	1161 (483, 3300)	18 (8, 23)	90.1/113
01me	1.66 (1.60, 1.73)	1.61 (1.34, 1.94)	6.4	0.3	5.67 (3.09, 8.09)	77 (40, 115)	277 (186, 451)	20 (15, 26)	32.5/41
02me	1.78 (1.73, 1.83)	2.49 (1.90, 4.10)	6.4	0.3	7.05 (2.90, 13.5)	76 (35, 99)	482 (198, 1165)	32 (17, 60)	8.89/21
15me	1.67 (1.64, 1.70)	2.30 (2.10, 2.52)	6.4	0.3	4.98 (2.49, 7.47)	48 (23, 72)	394 (290, 545)	27 (23, 32)	30.8/43
17me	1.75 (1.73, 1.79)	3.13 (2.83, 3.47)	6.4	0.3	6.13 (3.28, 8.93)	50 (27, 73)	419 (274, 621)	24 (18, 31)	30.6/43
o003	1.60 (1.57, 1.62)	1.98 (1.80, 2.17)	6.4	0.3	7.38 (4.96, 9.74)	73 (48, 98)	269 (243, 299)	25 (22, 28)	88.3/112
o392	1.63 (1.61, 1.65)	1.88 (1.76, 2.00)	6.4	0.3	3.41 (2.00, 4.79)	38 (22, 54)	268 (246, 293)	27 (25, 29)	65.1/66

NOTES.—The normalizations N_g and N_{line} have units of photons cm $^{-2}$ s $^{-1}$ keV $^{-1}$ and all errors are 90% confidence limits.

TABLE 4

FITS TO A MODEL OF GALACTIC ABSORPTION, POWER LAW WITH IONIZED REFLECTION, AND GAUSSIAN LINE

File Number	$\Gamma = \alpha + 1$	$\Omega/2\pi$	ξ	N_g	E_{line} (keV)	σ_{line} (keV)	$10^{-3}N_{\text{line}}$	EW (eV)	χ^2_{ν}/pha	χ^2_{ν} (diskline)
08	1.74 (1.66, 1.80)	0.31 (0.12, 0.5)	80 (0, 260)	1.54 (1.35, 1.76)	6.20 (5.95, 6.45)	0.62 (0.27, 1.05)	6.57 (2.7, 17)	97 (40, 245)	95.1/140	98.4
09	1.64 (1.62, 1.68)	0.56 (0.45, 0.71)	15 (0, 40)	1.43 (1.34, 1.49)	6.50 (6.40, 6.65)	0 (0.59)	2.34 (1.60, 6.0)	33 (22, 86)	96.6/106	96.3
10	1.61 (1.59, 1.63)	0.27 (0.18, 0.37)	62 (15, 160)	1.20 (1.15, 1.26)	6.50 (6.40, 6.59)	0 (0, 0.35)	2.46 (1.8, 3.7)	40 (30, 60)	88.4/115	88.9
13	1.82 (1.76, 1.87)	0.68 (0.44, 0.89)	61 (10, 110)	2.64 (2.35, 2.80)	6.32 (6.05, 6.50)	0.12 (0, 0.7)	2.77 (1.3, 10)	28 (15, 98)	163/169	163
14	1.73 (1.62, 1.81)	0.44 (0.16, 0.76)	91 (35, 195)	1.76 (1.48, 2.10)	5.81 (5.25, 6.30)	0.8 (0, 1.3)	7.3 (0.6, 25)	81 (16, 130)	85.6/113	89.9
01me	1.70 (1.64, 1.78)	0.67 (0.42, 0.95)	50 (5, 130)	1.30 (1.16, 1.49)	6.4	0.3	1.94 (0, 5.0)	32 (0, 81)	29.2/41	
02me	1.86 (1.79, 1.94)	0.99 (0.50, 1.55)	116 (0, 350)	1.77 (1.60, 2.00)	6.4	0.3	0.33 (0, 5.5)	5 (0, 85)	8.44/21	
15me	1.74 (1.70, 1.78)	0.85 (0.68, 1.05)	59 (10, 120)	1.76 (1.65, 1.91)	6.4	0.3	0.00 (0, 2.5)	0 (0, 32)	31.3/43	
17me	1.80 (1.77, 1.84)	0.70 (0.55, 0.88)	170 (80, 335)	2.39 (2.24, 2.54)	6.4	0.3	0.00 (0, 1.9)	0 (0, 20)	21.4/43	
o003	1.59 (1.56, 1.62)	0.59 (0.48, 0.71)	59 (13, 136)	1.37 (1.30, 1.43)	6.4	0.3	3.70 (1.5, 5.9)	48 (20, 78)	90.6/112	
o392	1.63 (1.61, 1.65)	0.75 (0.66, 0.84)	57 (30, 88)	1.27 (1.23, 1.32)	6.4	0.3	0.32 (0, 0.54)	5 (0.24)	55.7/66	

NOTES.—The last column gives the corresponding χ^2_{ν} for a similar model in which the Gaussian line is replaced by the diskline profile. The normalizations N_g and N_{line} have units of photons cm $^{-2}$ s $^{-1}$ keV $^{-1}$ and all errors are 90% confidence limits.

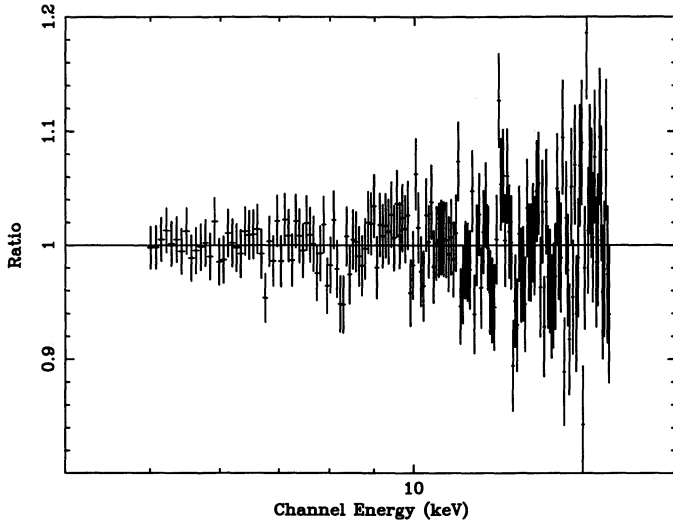


FIG. 2a

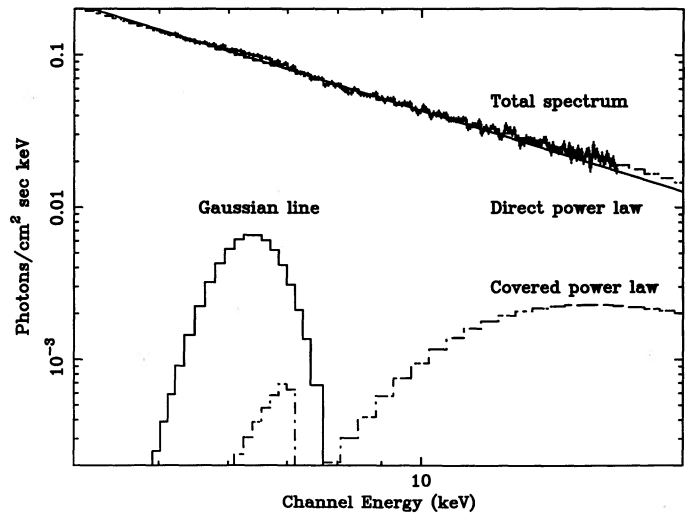


FIG. 2b

FIG. 2.—(a) Ratio of residuals (data/model) of a partial covering model (§ 5.2) to one of the GSPC spectra (13). A comparison with Fig. 1a shows that the inclusion of a line and high energy excess removes most of the systematic residuals. (b) Model spectrum.

1990). These are not overwhelming, with only one spectrum (*HEAO 1* day 392) giving reflection as over $100 \times$ more likely to be the correct description of the data. However, since these are independent data sets the likelihood ratio of the total set of results can be found from multiplication of the likelihood ratios (Edwards 1972, p. 11), giving that reflection is 3×10^7 more likely than partial covering to be the correct spectral form.

5.4. Power Law, Diskline and Reflection Spectrum

If the reflection is from an accretion disk, as assumed in the above model, the line profile should not be Gaussian but has a characteristic skewed shape from doppler boosting (suppression) of the blue (red) wing. Only the GSPC data can give any constraints on such line profiles, so here we refit these data using a diskline profile from an extreme Kerr

black hole as described in Laor (1992) to replace the Gaussian line profile in the fits described above. The line emissivity is parameterized as a power-law function with radius, $\propto r^{-q}$, where a point source at height h above the disk would be expected to have $q \sim 0$ for $r \ll h$, $q \sim 2$ for $r \sim h$ and $q \sim 3$ for $r \gg h$ if the disk is flat. As most of the line comes from the $r \sim h$ region (Matt et al. 1991), we fix $q = 2$. This line emissivity is then integrated over the area of the disk, from the inner to the outer radius, r_i and r_o respectively, with light paths following the full general relativistic geodesics to obtain the total line profile. The intrinsic iron line energy is restricted to between 6.4 and 6.67 keV, as implied by all the ionization parameters derived from the reflection spectra.

Despite these constraints, this extremely complex model is not able to provide significant restriction on the disk size even when the inner and outer radius of the disk were varied simul-

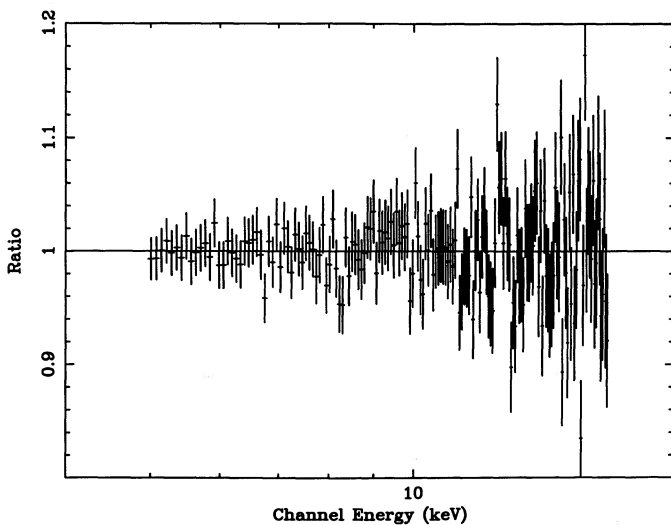


FIG. 3a

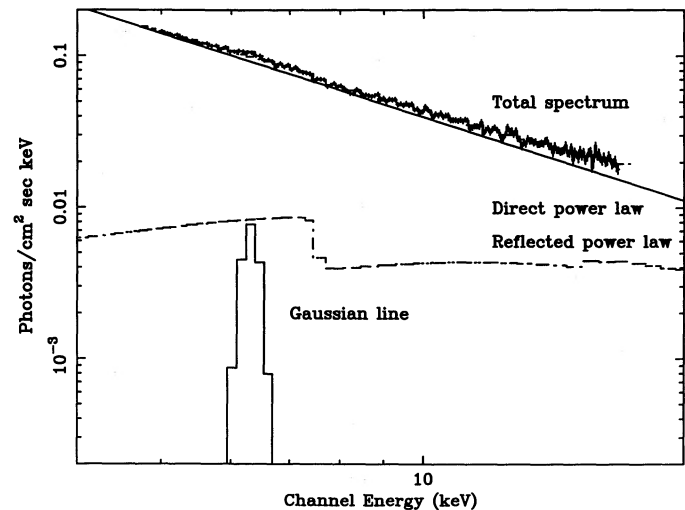


FIG. 3b

FIG. 3.—(a) Ratio of residuals (data/model) of a reflection model (§ 5.3) to one of the GSPC spectra (13); (b) Model spectrum. A comparison with Figs. 2a and 2b show that both partial covering and reflection give an acceptable fit to the data though the two models differ in their spectral form.

taneously in a 6×6 grid between 1.235–100 and $200\text{--}10^5$ gravitational radii, $R_g = GM/c^2$. As the line parameters are so ill constrained, and as the associated continuum parameter values are always consistent with those obtained in § 5.3, the fits are not tabulated here. The χ^2_ν values are given in Table 4. In three of the five spectra the fits are indistinguishable from those obtained with a Gaussian line, but in the remaining two the χ^2_ν is larger by $\Delta\chi^2_\nu \sim 4$ for the diskline profile from a Kerr black hole for the Gaussian line. The likelihood estimate can no longer be applied, as the number of parameters is not the same, but clearly the diskline is marginally (and probably not significantly) worse than a Gaussian profile in describing the data.

5.5. Sunyaev-Titarchuk Comptonized Spectrum, Reflection and Line

The continuum spectrum of Cyg X-1 is generally fit at $E \geq 30$ keV by a thermal Compton form (Sunyaev & Titarchuk 1980). These fits typically have values of temperature and optical depth in the range $kT = 27\text{--}60$ keV and $\tau = 1\text{--}5$ (see the review of Liang & Nolan 1984). Here we look at the applicability of these models to the lower energy data, and examine how sensitive the derived parameters are to the presence of reflection.

Only the *HEAO 1* data were used, as the parameters of a thermal Compton spectrum are most sensitive to the high-energy spectral shape. Where reflection is included, the power-law flux illuminating the disk is fixed to the best-fit spectral index in § 5.3, and its normalization tied to that of the Sunyaev-Titarchuk thermal Compton spectrum, but the ionization parameter and solid angle were free to vary.

Without reflection, the fits to the data are poor. The derived temperatures are low, with $kT \sim 15$ keV, and the corresponding optical depth is high $\tau \sim 6.5$. The reflection spectrum, with its peak at ~ 20 keV, is driving the continuum fit. When reflection is included the continuum temperature increases to $kT > 45$ keV on day 003, and $kT > 67$ keV on day 392, with corresponding limits on the optical depth of $\tau < 3.37$ and $\tau < 2.53$. The temperatures are only lower limits as the *HEAO 1* spectra extend only to 50 keV so cannot constrain high temperature models as they are identical (within the errors) to a power law over this energy range. The derived parameters for the reflection spectrum and Gaussian line are consistent with those found for the power-law fits § 5.3, so are not repeated here. The χ^2_ν values are identical also, showing that the data cannot distinguish between a power law and high-temperature thermal Compton continuum. However, the 90% confidence limit on the temperature for day 392 is higher than any previously tabulated value (Liang & Nolan 1984; Ling et al. 1987) suggesting that either the high-energy fits are affected by the reflection spectrum or that the continuum spectrum is not a single-temperature thermal Compton spectrum. The latter possibility is favored as the temperature is very well defined in the high-energy data where the exponential rollover in the spectrum is seen. There is also evidence for a multicomponent spectrum from the observation of an intermittent, hard, very high energy (0.5–2 MeV) spectrum in Cyg X-1 (Liang & Dermer 1988). Multitemperature thermal Compton components, or a relativistic Compton spectrum are probably a better description of the continuum form.

5.6. Summary of Spectral Fits

We find that the best fits to the Cyg X-1 data from both the *EXOSAT* instruments and the *HEAO 1*-A2 HED data are

consistent with a Compton reflection model and that as a whole the data are significantly better described by this than by a partially covered model. Diskline fits to the Fe line are not significantly better than Gaussians and the line energy and width are consistent with being at 6.4 keV and unbroadened respectively in all but one of the five spectra. The underlying form of the continuum is not better fit by a Sunyaev-Titarchuk thermal Compton model of temperature less than 60 keV than by a power law.

6. DISCUSSION

Cyg X-1 is widely believed to be a black hole/accretion disk system. If this interpretation is correct then a Compton reflection spectrum and reprocessed iron fluorescence line with skewed profile are expected to contribute to the continuum emission. The addition of a reflection spectrum and Gaussian line to a power-law continuum model give excellent fits ($\chi^2_\nu/\nu \leq 1$) to archival data from *EXOSAT* and *HEAO 1*-A2. These are generally better than the fits to the partially covered power-law model, and the sample of 11 spectra together are significantly more likely to have a reflected power law than a partially covered spectrum as the high-energy excess.

6.1. Amount of Reflection

As explained in § 4, the amount of reflection seen is dependent on the geometry of the reflector, its ionization state, abundance, and inclination and also on the geometry of the source. For Cyg X-1, the inclination is well constrained, the abundance is known for Fe as $\sim 2 \times$ solar and for the other elements as not differing from solar by a large factor, and the ionization state can be directly measured from model fitting. This leaves the only free parameters as the source and disk geometry. Here we try to constrain these from the amount of reflection seen.

Three possible source geometries are considered, namely a central, optically thick source, an extensive corona and a point source (equivalent to a small corona) above a disk. Where the disk is flat and of solar abundance these predict a normalization of $\Omega/2\pi \approx 0.5, 1.0,$ and $1.5,$ respectively (see Appendices). Increasing the elemental abundances gives an approximately linear decrease in the normalization (George & Fabian 1991) whereas increasing the solid angle subtended by the material gives an approximately linear increase in the normalization (Matt et al. 1991).

Note that the extensive corona is only included for completeness as there is independent evidence that the X-ray source is not extended over much of the disk: the *Tenma* data during a prolonged dip suggest that the hard X-ray source is completely covered by the clumpy stellar wind material but that the soft X-rays, presumably from the disk, are not. On these grounds the point source (or small corona) and central, optically thick source are favored. Both of these have a strong theoretical basis. A small source is produced in nonthermal acceleration models (see, e.g., Blandford & Znajek 1978) and also in calculations of thermal coronae (Begelman, McKee, & Shields 1983), whereas a central, optically thick source is produced in some theoretical models of accretion disks (Shapiro, Lightman, & Eardley 1976).

6.1.1. Amount of Reflection and Behavior with Phase

Figures 4a and 4b show the solid angle obtained from the fits to the model of absorption, power law, reflection and line (§ 5.3) plotted against the 5.6 and 294 day phase. These give $\Omega/2\pi = 0.57 \pm 0.07$ (error is 1σ) with $\chi^2_\nu = 18.51$ for 10 degrees of freedom, which cannot exclude a constant value at more

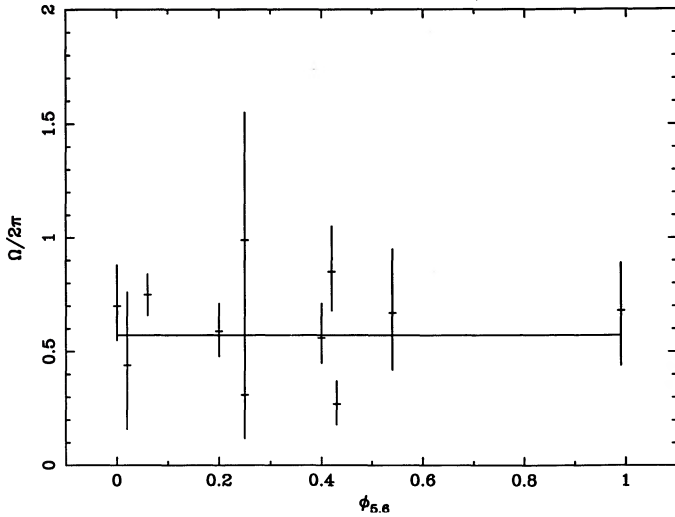


FIG. 4a

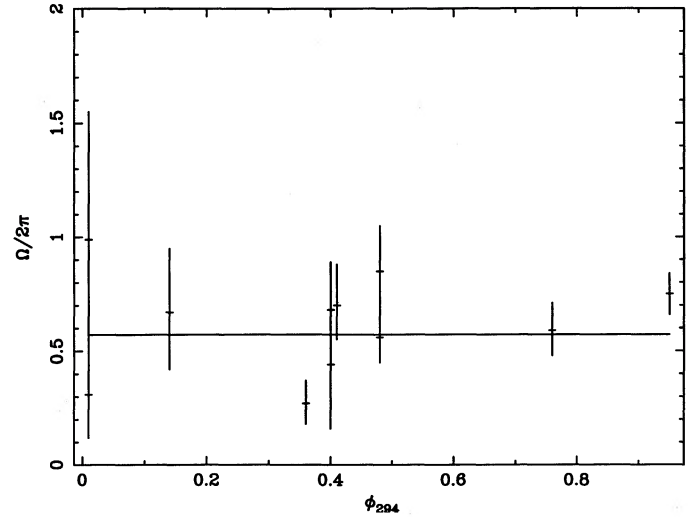


FIG. 4b

FIG. 4.—Solid angle $\Omega/2\pi$, subtended by the reflecting material (§ 5.3) shown as (a) a function of binary phase (5.6 days) and (b) as a function 294 day phase. The scatter of the solid angle shows no obvious trend with either phase, and is consistent with being constant at the 5% probability level, of $\Omega/2\pi = 0.57 \pm 0.07$ with $\chi^2 = 18.51$ for 10 d.o.f.

than 95% confidence level. There is no readily apparent trend with either phase. If the 294 day period is related to precession of the accretion disk then some change in apparent solid angle is expected to arise from the change in inclination of the disk. However, this is small (Merritt & Petterson 1980), and would not be detectable in this study.

For solar abundances, the small value of the normalization immediately rules out all solutions except that of a spherical, optically thick source at the center of a flat disk, or a physically small disk, whose horizontal extent was not substantially larger than the vertical distance of the point source or corona. A small disk seems unlikely (though cannot be ruled out from the diskline fits § 5.4), as both the self-gravitation or tidal disruption radii (which give a physical explanation for the finite size of the disk) are extremely large (Kemp 1980). A funnel-like, or flared disk, with their even larger solid angles are definitely not consistent with the data under these assumptions.

6.1.2. Constraints on Geometry: Fe $2 \times$ Solar

The above discussion of solar abundances is probably not applicable to Cyg X-1 as X-1, earlier *Tenma* data indicate that $\text{Fe}/\text{H} = 6 \pm 1 \times 10^{-5}$, i.e., twice cosmic abundance. This depresses the reflection spectrum past the iron edge by roughly 70% (Lightman & White 1988), leading to a prediction of $\Omega/2\pi \sim 0.9, 0.7$, and 0.45 for a point source, extensive corona, and central optically thick source, respectively. Again the central, optically thick source is the only solution within 3σ of the observed normalization.

6.1.3. Constraints on Geometry: All Elements at Enhanced Abundance

Increasing the abundances of the other elements, such as C, N, and O, is a way to further depresses the reflection spectrum. Large abundance enhancement through nuclear reprocessing is unlikely, as HDE 226868 is still in the hydrogen core burning stage (Conti 1978), whereas material enriched by the CNO cycle does not migrate outwards until the He burning stage (Maeder & Meynet 1987). Evolutionary scenarios for such massive close binaries also support this conclusion (Doom & de Greve 1983). However, this does not rule out factors of a few

enhancement in the initial abundance of the system, as indeed seen in the iron abundance (Kitamoto et al. 1984).

A point source above a flat disk of $\sim 3 \times$ solar abundances of all the elements leads to a predicted normalization of $\Omega/2\pi = 0.5$, as does an extensive corona above a flat disk of twice solar abundance. The central, optically thick source predicts $\Omega/2\pi = 0.37$ for twice solar abundances and so requires the material to subtend a solid angle larger by $\sim 50\%$ than a flat disk in order to bring the normalization up to the observed value.

6.2. Iron $K\alpha$ Line

The line must be consistent with the proposed disk geometry. Only the GSPC data have high enough spectral resolution to give information on this. For a point source above a flat disk (inner radius of $5R_s$, outer radius of $500R_s$, and height of source above the disk is $10R_s$, where the Schwarzschild radius, $R_s = 2GM/c^2$) inclined at 30° , the expected line energy and width are ~ 6.2 and ~ 0.5 keV, respectively (Matt et al. 1992). A weighted average of the data in Table 4 gives a mean energy of 6.44 ± 0.12 keV and width of $0.27^{+0.31}_{-0.27}$ keV, both within 3σ of the predicted values. However, in two individual GSPC spectra the 90% confidence contours for the line energy exclude the value of 6.2 keV, requiring that Fe be highly ionized (He-like), such that the line is preferentially emitted at 6.67 keV.

Fits with the diskline profile are not significantly better than the Gaussian line profile, and some fits are marginally worse (see Table 4). If significant, this may be explained if the line is a composite of both the expected diskline and a Gaussian line from fluorescence from the stellar photosphere and wind. The stellar component is expected to contribute 10–20 eV in equivalent width to the Fe $K\alpha$ line (Basko 1978; Kitamoto et al. 1990), giving a composite line with a Gaussian core added to the skewed profile, distorting the diskline fits. This argument can be used if the disk is flat, but if the disk is flared, then the star may be shielded from the X-ray irradiation. However, this would still result in a poor fit with the diskline profile models as the line emissivity for a flared disk is different from that of a

flat disk, with more line arising from the outer, low-velocity, region. We stress that better spectral resolution is required to draw firm conclusions from the line profile. However, there are indications in AGN spectra that a diskline profile is not an adequate description of the data (Pounds 1992), suggesting that there may be a discrepancy between present models and observations.

6.3. Ionization State of the Reflecting Material

The best-fit reflection spectrum is always indicative of ionized material. This is driven by the Fe edge energy, that is required by the data to be at energies larger than 7.1 keV. The model assumes that this energy shift is due to photoionization of the material, which should produce a linear correlation between the ionization parameter and luminosity. These data are shown in Figure 5. While the data are consistent with such a correlation, the large error bars on the parameters mean it is not required.

As this conclusive test cannot be performed with these data, we examine other possibilities for the energy shift of the edge. Collisional ionization cannot give the observed ionization state as only the very innermost regions of the disk have the high temperature ($kT \sim 0.3$ keV) required for Fe xv (Makashima 1986). There is a possibility that the disk kinematics (not modeled here) can lead to such an apparent energy shift (see Matt et al. 1991, and the Appendices). However, we think such an effect unlikely to be seen in spectral fitting with moderate resolution detectors, and the requirement that the line arise from ionized material in two of the five GSPC spectra seems to confirm this.

Assuming then that photoionization is the most probable interpretation, this requires that the material be close to the X-ray source and not so dense that it can cool through bremsstrahlung (free-free) emission. At an inclination of 30° , half of the reflected photons come from within $50R_g$ (Matt et al. 1991), so the mean ionization state will correspond to the density and temperature at this point. Note that for a flared disk the larger

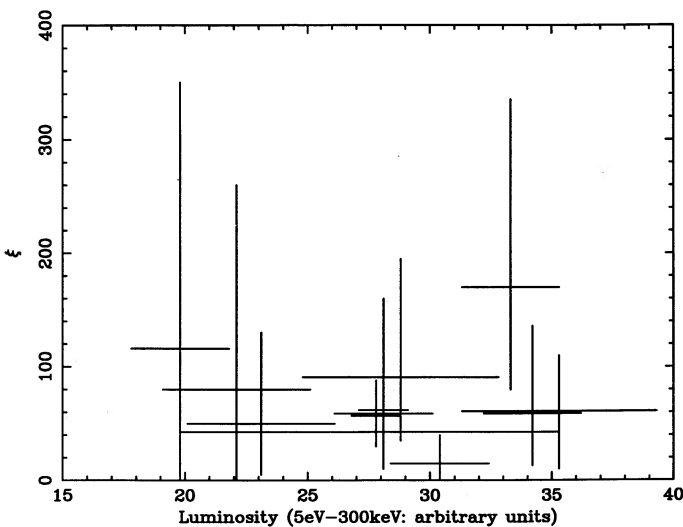


FIG. 5.—Ionization parameter, $\xi = L/nR^2$, from the fits in § 5.3, plotted against the extrapolated power-law flux integrated between 5 eV and 300 keV, i.e., $\propto L$. The expected correlation is consistent with the data, but the large error bars on both quantities mean that it is not required. The data are sufficiently well described by a constant, with $\xi = 42.7 \pm 26$, $\chi^2 = 2.7$.

solid angle at larger radii increases the half-reflection point. Taking a mean X-ray luminosity of $\sim 10^{38}$ ergs s^{-1} so the source is running at approximately 10% of Eddington for $M = 10 M_\odot$, the weighted mean value of $\xi \sim 40$ implies $N_e R^2 \sim 2 \times 10^{36} \text{ cm}^{-1}$, where N_e is the disk density and R is the mean distance of the X-ray source from the reflecting material. For a standard Shakura-Sunyaev disk (see e.g., the collated equations in Laor & Netzer 1989), a density of $N_e \sim 3.5 \times 10^{20} \text{ cm}^{-3}$ at this radius, requires a viscosity of $\alpha \sim 2$.

The estimate of the disk density is an upper limit. At such high densities, three body recombination becomes an important factor (H. Netzer 1991, private communication). The neglect of this term means that the recombination rate is underestimated, so the fact that such a high ionization state is seen implies that the density of the material is lower than calculated above. As the viscosity is inversely proportional to the density, the value of $\alpha \sim 2$ derived above is an *underestimate*. But it is usually taken that $\alpha = 1$ is the upper value, limited by the onset of turbulence. Hence it seems unlikely that the standard Shakura-Sunyaev disk equations can be used to describe the disk in Cyg X-1 if the disk is flat. The flared disk, with its larger half reflection radius predicts even larger values for α , making it even more unlikely that the disk viscosity is proportional to the total (gas plus radiation) pressure.

6.4. Line Equivalent Width

There are some remaining problems with the model as described. Figure 6 shows the line equivalent width from the GSPC spectra as a function of binary (5.6 day) phase. The *HEAO 1* and ME data on the line are excluded as the fixed line energy and width may have affected the limits on the equivalent width. The line equivalent width is consistent with a constant, at 44 ± 28 eV. The line expected from a point source above a flat, solar abundance disk (inner radius of $5R_g$, outer radius of $500R_g$, and height of source above the disk is $10R_g$) inclined at 30° , is 140 eV (Matt et al. 1992). So that from a spherical optically thick source is ~ 70 eV (Matt et al. 1991). For a disk ionized up to Fe xv the decrease in opacity of the disk material increases the probability that the line photons

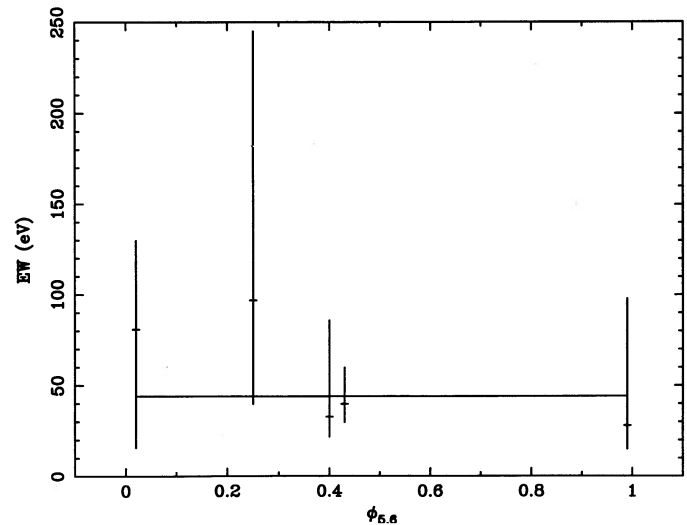


FIG. 6.—Equivalent width of the Gaussian line (EW) from the fits in § 5.3 plotted against binary phase (5.6 days). The line intensity is consistent with a constant, with $EW = 44 \pm 28$ eV.

can escape from the disk (i.e., give the observed $K\alpha$ line) by $\sim 50\%$, increasing the expected line equivalent widths to 210 and 105 eV for the point source and spherical source, respectively. Note that the assumption of a single ionization state for the disk is obviously inaccurate as the inner disk regions will be more highly ionized than the outer regions. Detailed Monte Carlo calculations are required to treat this effect properly, but are beyond the scope of this paper.

The possible scenarios to account for the amount of reflection seen are given in § 6.1. A point source above a disk which is a factor of 3 overabundant in all the elements, gives a final expected line of 210 eV (see Appendix E). Subtracting 10–20 eV from the equivalent width as being due to the star and stellar wind, the observed data is more than 5σ below this prediction. Likewise, the spherical source at the center of a flat disk in which only iron is overabundant predicts a line of 210 eV (see Appendix E), again more than 5σ above that observed. Increasing the abundance of the other elements by a factor of 2 reduces the expected line to 105 eV but the disk is then required to be flared to take the solid angle from $\Omega/2\pi$ of 0.38 to 0.57. As detailed calculations of the line have not been done for this geometry, we simply scale the line with the solid angle, increasing the expected equivalent width to 157 eV. This is the smallest predicted line, and gains also by the fact that a flared disk may shield the star from the X-ray flux, reducing the line from the star and wind. This gives the smallest discrepancy between the predicted and observed line equivalent width in all of the scenarios, being $\sim 3\sigma$ above that observed, it is still systematically higher than the data. Even if the ionization state of the disk is overestimated due to doppler blueshifts (see Appendix F), the smallest predicted line is 105 eV (flared disk). A very small line equivalent width is also seen in Cyg X-1 by Kitamoto et al. (1990) in *Tenma* data, including one observation in which the upper limit on the line was ≤ 38 eV.

This may be a problem for the standard accretion disk models as they stand at present. Reflection without substantial line emission is also seen in the bright low-mass X-ray binary systems X1608, X1636, X1254, and Cyg X-2 (Mitsuda 1992), and also in the black hole candidate GS 2000+25 (Ebisawa 1991). This lack of direct correlation between the line equivalent width and reflection spectrum normalization suggests that there may be a widespread problem in the illuminated accretion disk models in X-ray binary systems.

6.5. Intrinsic Properties of the X-ray Source

There is much circumstantial evidence that the X-ray source is marginally optically thick, whatever its shape or emission mechanism. Thermal Comptonization model fits to the spectrum of Cyg X-1 require $\tau_{es} \geq 2$ (Sunyaev & Titarchuk 1980; Liang & Nolan 1984; § 5.5), and nonthermal models probably involve pair production, which, at the high efficiency of Cyg X-1, result in a cooled population of pairs of similar optical depth to the thermal models (Fabian et al. 1986).

The weighted mean intrinsic spectral index is $\alpha = 0.66 \pm 0.02$, but with $\chi^2_\nu = 4.9$ is not consistent with a constant (see Fig. 7). Neither is a linear correlation with luminosity a significantly better fit. The scatter is apparently random. As these spectral indices are already corrected for the effects of reflection, this should give information about the emission process itself.

The random scatter in the spectral index rules out a simple interpretation of the variability. In either thermal or non-thermal models for the X-ray emission, equilibrium states

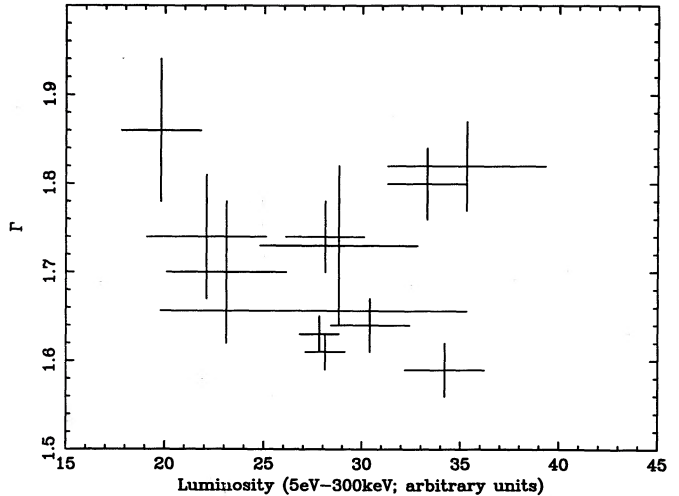


FIG. 7.—Intrinsic spectral index vs. the luminosity of the source. The spectral index is not constant, but shows random scatter about the mean of $\Gamma = 1.66 \pm 0.02$ ($\chi^2 = 49.15$ for 10 d.o.f.) rather than a systematic trend.

(applicable to Cyg X-1 because the time scales controlling the physical processes are very much shorter than the observation length) give a systematic rather than random change in spectral index for variability of one parameter (see, e.g., thermal: Sunyaev & Titarchuk 1980; nonthermal: Fabian et al. 1986).

7. SUMMARY

The 5–50 keV spectrum of Cyg X-1 clearly shows evidence for the high-energy excess seen in AGNs. This can be well fit by both partial covering models and by reflection, but we find that reflection is considerably more likely than the partial covering to be the correct description of the data in Cyg X-1. This is the first time that the reflection model has been shown to be a better fit, and on data which provide the best test to date of reflection due to the high-energy extent of the *HEAO 1-A2* data. That the reflected spectrum is constant over long periods of time implies that the disk is long-lived and stable, in contrast to the short disk formation/destruction cycle expected in a pure wind accretion system, and favoring the focused wind accretion theories.

The observed reflection spectrum depends on the intrinsic source spectrum, source and disk geometry, and the temperature, density, and elemental abundances of the disk. In Cyg X-1 there is independent evidence that the iron abundance is twice cosmic and that the X-ray source geometry is unlikely to be an extensive corona over the whole disk. The reflection spectrum is only 70% of that expected from a flat disk of twice cosmic iron abundance illuminated by a point source or small corona but is consistent with that expected from point source above a disk where all the elements are more than twice cosmic abundance. The reflection is also consistent with a spherical, optically thick source at the center of either a flat disk where only iron is overabundant, or a flared disk where all the elements are overabundant.

The disk is ionized, with the mean ionization state corresponding to Fe xv. In a standard Shakura-Sunyaev disk (viscosity \propto total pressure), this gives a disk density of less than $\sim 3 \times 10^{20} \text{ cm}^{-3}$, corresponding to a viscosity parameter $\alpha \geq 2$. As turbulence limits the viscosity to $\alpha \leq 1$ it seems unlikely that the standard Shakura-Sunyaev equations are

valid. With better data, this technique may be able to observationally constrain the theories of disk structure.

However, the strength and shape of the Fe line presents the one obstacle to a completely self-consistent picture, where the line and reflection spectrum arise from an X-ray illuminated accretion disk. Firstly, while the line is consistent with the skewed profile expected from the ordered angular momentum structure of the disk, there may be indications that the Gaussian line profile is a better fit. There are several possible explanations for the effect, if real. Contamination of the diskline profile from the more Gaussian line emission from the stellar surface and wind, or a nonflat disk geometry would both produce a distortion of the line profile from that expected. Intriguingly, there are indications that the same effect is seen in some AGNs (Pounds 1992) where a purely stellar explanation cannot apply, favoring the flared disk geometry.

The line equivalent width is also discrepant. The three geometries described above, which are consistent with the amount of reflection seen, all predict a larger line equivalent width than is observed, though a spherical source at the center of a flared disk where the elemental abundances are around twice cosmic predicts a line which is less than 3σ from the observed value. The discrepancy is important as the normal-

ization of the reflection spectra is strongly linked to the depth of the edge in the data, which is causally linked to the line. To see a large reflection spectrum (i.e., large edge) and not see the accompanying iron line emission may be a more widespread problem as four other X-ray binaries show the same disquieting trend. While it may be indicative of the local abundance variations postulated in the flared disk model, it may also be a pointer to a more fundamental problem in our understanding of the nature of these sources.

The reflection code will be made available to the astronomical community under the XSPEC X-ray spectral fitting package.

C. D. acknowledges receipt of a National Research Council-GSFC Research Associateship. We thank Nick White and Lorella Angelini for many helpful discussion of *EXOSAT* instrumental effects, Tim Kallman for providing the machine readable atomic cross section data and for many helpful discussions, and Mike Corcoran and Andy Pollock for all the stellar evolution/abundance information. Thanks are due to the *EXOSAT* data base team, for their excellent archive from which most of the data for this paper was taken.

APPENDIX A

COMPTON REFLECTION FROM COLD MATERIAL

A semi-analytic form using Greens functions to calculate the reflection spectrum from a semi-isotropically illuminated flat disk is given by Lightman & White (1988) and White, Lightman, & Zdziarski (1988). At low energies the Greens function is a δ function, dependant on the photoelectric opacity of the disk, whereas at higher energies Compton downscattering requires that the reflection spectrum be calculated by an integral of the Greens function with the incident spectrum, which we assume to be a power law extending to 300 keV, consistent with high-energy observations (Liang & Nolan 1984). These two approximations are matched at 15 keV but the model spectrum is not quite smooth at this point as the gradient is discontinuous. This small effect can be seen in the comparison of this analytic calculation with Monte Carlo spectra (George & Fabian 1991). The assumed cutoff at 300 keV has little effect on the shape of the total spectrum because of the turndown in the reflection spectrum at high energies.

APPENDIX B

COMPTON REFLECTION FROM IONIZED MATERIAL

As the accretion disk may be close to the X-ray source, the material could be ionized (Begelman & de Kool 1992). This changes the photoelectric absorption opacity and hence the probability of reflection for low-energy photons. The population levels are calculated by equating the photoionization rate with the recombination rate for the reaction $X^i + \gamma \rightarrow X^{i+1} + e$ (see, e.g., Osterbrock 1989). Here we make the simplifying assumptions that radiative transfer is not important and that the power-law spectrum extends unbroken from $h\nu_{\min} = 5$ eV (below the ionization potential of 7 eV for neutral Fe and Mg) to the assumed spectral cutoff at $h\nu_{\max} = 300$ keV. Again, the exact cutoff value is not important as it has very little effect on the ion populations because of the ν^{-3} behavior of the photo-electric cross-sections. We also only consider the elements H, He, C, N, O, Ne, Mg, Si, S, and Fe, with abundances given in Lang (1974). Then the population levels are given by

$$\frac{N(X^{i+1})}{N(X^i)} = \frac{1}{\alpha(X^{i+1})} \frac{L}{N_e R^2} \int_{\nu_{\min}}^{\nu_{\max}} \frac{f_\nu}{4\pi h\nu} \sigma_\nu(X^i) d\nu$$

where $N(X^i)$ is the number density of the i th ionization state of element X , N_e is the number density of electrons, $L_\nu = Lf_\nu$ is the luminosity in $\text{ergs s}^{-1} \text{Hz}^{-1}$ at frequency ν , σ_ν is the photoelectric cross section, α is the recombination rate and R is the distance from the source to the ionized material. Recombination rates and photoionization rates are taken from Shull & Van Steenburg (1982) and Reilman & Manson (1979), respectively, for all ion states apart from hydrogenic where the analytic formulas are used (see, e.g., Osterbrock 1989). The cross sections given by Reilman & Manson (1979) are extrapolated with a ν^{-3} power law above 5 keV where their tabulation ends. Recombination is a weak function of temperature, so this must be chosen appropriately for the object considered, and must be between 10^3 – 10^6 K for the approximation used. Defining $\xi = L/(N_e R^2)$, where L is then the integrated luminosity between 5 eV and 300 keV, then the definition of the ionized disk reflection spectrum is similar to that for the cold disk with only two additional parameters, ξ and T .

The assumption that the luminosity is given by an extrapolation of the power-law emission minimizes the total ionizing flux. In Cyg X-1 the thermal emission from the disk itself contributes a “soft excess,” which can far exceed the power-law emission below 1 keV. This will ionize light elements much more efficiently than the power law, but has little effect on the high energy reflection spectrum, from the Fe edge and above. This is because the Fe ion population and high energy excess are driven by the high-energy photons, preferentially the hard power-law emission. As fitting reflection spectra in the 5–50 keV range is driven by the Fe edge and high-energy excess, the neglect of the soft component is justified.

APPENDIX C

EFFECT OF GEOMETRY OF THE SOURCE

The amount of reflection is also dependent on the geometry of the X-ray source itself. Reflection occurs from approximately a mean Thomson scattering optical depth, τ_{es} , of unity but the probability of the photon emerging after reflection is determined by the *absorption* optical depth in the direction to the observer. For a semi-isotropically illuminated disk, the incidence angle of the radiation onto the disk is $\sim 90^\circ$ so the photons penetrate a vertical depth of $\tau_{es} \sim 1$ into the disk. For a centrally concentrated source the weight mean incidence angle of the primary radiation, $\langle \theta \rangle$, is smaller, so the vertical depth is only $\tau_{es} = \cos \langle \theta \rangle$, allowing more photons to escape in all directions as the absorption opacity to the surface is correspondingly smaller. Thus a point source gives a reflection spectrum $\approx 50\%$ larger below 15 keV (see Figs. 11 and 12 in George & Fabian 1991) than that of an extended corona.

APPENDIX D

EFFECT OF GEOMETRY OF THE REPROCESSOR

To zeroth order the amount of reflection spectrum seen will scale with the solid angle subtended by the disk at the X-ray source, $\Omega/2\pi$. Thus a flared disk will give more reflection than a flat disk. This simple picture is qualitatively correct, and is the parameterization used in the model. Quantitatively, however, it is modified by several effects. When the disk is flared then some parts of the reprocessing surface may be hidden from the observer by the outer parts of the disk. Also a flared disk may reflect the reflected radiation as well as the primary emission (see Matt et al. 1991). We neglect these effects in our modeling of the amount of reflection observed.

The inclination, θ , of the reflection system to the observer is also an important parameter as it determines the path length (optical depth) through the material after scattering. The probability for escape is then $\propto e^{\cos \theta}$. However, the nonisotropic nature of the Compton scattering cross section means that this is not an exact description of the angular distribution of the reprocessed radiation (George & Fabian 1991; Matt et al. 1991). Hence a cosine dependence is used, which is within 15% of the numerical calculations at 30° (the inclination of Cyg X-1, Gies & Bolton 1986).

APPENDIX E

EFFECT OF METAL ABUNDANCE

As the escape probability is dependent on the absorption opacity, the abundance is also an important factor in determining the amount of reflection. If the abundance of all the elements is increased (decreased), then the reflection spectrum decreases (increases) by roughly the same factor but the equivalent width of the Fe $K\alpha$ fluorescence line remains much the same as that for cosmic abundance material (George & Fabian 1991). Although the number of line photons increases (decreases), so their probability of escape decreases (increases) and these two effects cancel almost exactly.

APPENDIX F

RELATIVISTIC EFFECTS

A subtle effect, not included in our code, is the change in shape of the reflection spectrum below 20 keV with inclination angle, both intrinsically and through relativistic and kinematic effects. Intrinsically, the peak of the reflection spectrum decreases from 15 to 12 keV as the inclination of the disk increases (Matt et al. 1991) because of the increased opacity. Relativistic and kinematic effects have most effect on the spectral features, giving the line a distinctive profile from doppler effects (Fabian et al. 1989; Matt et al. 1992; Laor 1992) and smearing the edge (Matt et al. 1991). The minimum in the resultant smeared edge is blueshifted, just as the maximum peak of the line is blueshifted. Matt et al. (1991) point to this as a possible danger; that these doppler effects can mimic absorption by higher ionization states of iron. However, the overall weighted line centroid is always *redshifted* at moderate inclinations, so we expect that a weighted edge energy (which is in effect what is measured by spectral fitting with moderate resolution detectors) would be similarly redshifted, lessening confusion between ionization and doppler effects.

REFERENCES

- Allen, C. W. 1973, *Astrophysical Quantities*, 3rd ed. (London: Athlone)
- Awaki, H. 1990, Ph.D. thesis, Nagoya Univ.
- Balucinska, M., & Barr, P. 1992, in *Iron Line Diagnostics in X-Ray Sources*, ed. A. Treves (Berlin: Springer), in press
- Balucinska, M., & Hasinger, G. 1991, *A&A*, 241, 439
- Barr, P., & Van der Woord, H. 1990, *ApJ*, 352, L41
- Barr, P., White, N. E., & Page, C. G. 1985, *MNRAS*, 216, 65P
- Basko, M. M. 1978, *ApJ*, 223, 268
- Begelman, M. C., & de Kool, M. 1992, *Proc. of the Conference on Variability of Active Galactic Nuclei*, ed. H. Miller & P. Wiita (Berlin: Springer), in press
- Begelman, M. C., McKee, C. F., & Shields, G. A. 1983, *ApJ*, 271, 70
- Blandford, R. D., & Znajek, R. L. 1977, *MNRAS*, 179, 433
- Chen, K., & Halpern, J. P. 1989, *ApJ*, 344, 115
- Conti, P. S. 1978, *A&A*, 63, 2
- Doom, C., & de Greve, J. P. 1983, *A&A*, 120, 97
- Ebisawa, K. 1991, Ph.D. thesis, Univ.
- Edwards, A. W. F. 1972, *Likelihood* (Cambridge: Cambridge Univ. Press)
- Fabian, A. C., Blandford, R. D., Guilbert, P. W., Phinney, E. S., & Cuellar, L. 1986, *MNRAS*, 221, 931
- Fabian, A. C., Rees, M. J., Stella, L., & White, N. E. 1989, *MNRAS*, 238, 729
- Friend, D. B., & Castor, J. I. 1982, *ApJ*, 261, 293
- George, I. M., & Fabian, A. C. 1991, *MNRAS*, 249, 352
- Gies, D. R., & Bolton, C. T. 1986, *ApJ*, 304, 371
- Guilbert, P. W., & Rees, M. J. 1988, *MNRAS*, 233, 475
- Kallman, T. 1986, in *The Physics of Accretion onto Compton Objects*, ed. K. O. Mason, M. G. Watson, & N. E. White (Berlin: Springer), 269
- Kallman, T., Stevens, I. R., & Blondin, J. 1992, *ApJ*, in press
- Kemp, J. C. 1980, *ApJ*, 235, 595
- Kitamoto, S., Miyamoto, S., Tanaka, Y., Ohashi, T., Kondo, Y., Tawara, Y., & Nakagawa, M. 1984, *PASJ*, 36, 731
- Kitamoto, S., Takahashi, K., Yamahita, K., Tanaka, Y., & Nagase, F. 1990, *PASJ*, 42, 85
- Lang, K. R. 1974, *Astrophysical Formulae* (New York: Springer)
- Laor, A. 1992, *ApJ*, submitted
- Laor, A., & Netzer, H. 1989, *MNRAS*, 238, 897
- Li, F. K., & Clark, G. W. 1974, *ApJ*, 191, L27
- Liang, E. P., & Dermer, C. D. 1988, *ApJ*, 325, L39
- Liang, E. P., & Nolan, P. L. 1984, *Space Sci. Rev.*, 38, 353
- Lightman, A. P., & White, T. R. 1988, *ApJ*, 335, 57
- Ling, J. C., Mahoney, W. A., Wheaton, W. A., & Jacobson, A. S. 1987, *ApJ*, 321, L117
- Maeder, A., & Meynet, G. 1987, *A&A*, 182, 243
- Makashima, K. 1986, in *The Physics of Accretion onto Compact Objects*, ed. K. O. Mason, M. G. Watson, & N. E. White (Berlin: Springer), 250
- Mason, K. O., Hawkins, F. J., Sanford, P. W., Murdin, P., & Savage, A. 1974, *ApJ*, 192, L65
- Matsuoka, M., Yamauchi, M., Piro, L., & Murakami, T. 1990, *ApJ*, 361, 440
- Matt, G., Perola, G. C., & Piro, L. 1991, *A&A*, 247, 25
- Matt, G., Perola, G. C., Piro, L., & Stella, L. 1992, *A&A*, submitted
- McClintock, J. E. 1986, in *Physics of Accretion onto Compton Objects*, ed. K. O. Mason, M. G. Watson, & N. E. White (Berlin: Springer), 211
- Merritt, D., & Petterson, J. A. 1980, *ApJ*, 236, 255
- Mitsuda, K., 1992, in *Proc. 28th Yamada Conference, Frontiers of X-ray Astronomy*, ed. K. Koyama & H. Kunieda (Tokyo: Universal Academy Press), in press
- Miyamoto, S., & Kitamoto, S. 1989, *Nature*, 342, 773
- Mushotzky, R. F. 1982, *ApJ*, 256, 92
- Nandra, K., Pounds, K. A., Stewart, G. C., Fabian, A. C., & Rees, M. J. 1989, *MNRAS*, 236, 39P
- Osterbrock, D. E. 1989, *Astrophysics of Gaseous Nebulae and Active Galactic Nuclei* (Mill Valley, CA: University Science Books)
- Parmar, A. N., & Izzo, C. 1986, *EXOSAT Express*, 16, 21
- Piro, L., Yamauchi, M., & Matsuoka, M. 1990, *ApJ*, 360, L35
- Pounds, K. A. 1992, in *Proc. 28th Yamada Conference, Frontiers of X-ray Astronomy*, ed. K. Koyama & H. Kunieda (Tokyo: Universal Academy Press), in press
- Pounds, K. A., Nandra, K. A., Stewart, G. C., George, I. M., & Fabian, A. C. 1990, *Nature*, 344, 132
- Pounds, K. A., Nandra, K. A., Stewart, G. C., & Leighly, K. 1989, *MNRAS*, 240, 769
- Pravdo, S. H., White, N. E., Kondo, Y., Becker, R. H., Boldt, E. A., Holt, S. S., Serlemitsos, P. J., & McCluskey, G. E. 1980, *ApJ*, 237, L71
- Priedhorsky, W., Terrel, J., & Holt, S. S. 1983, *ApJ*, 270, 233
- Reilman, R. F., & Manson, S. T. 1979, *ApJS*, 40, 815
- Robinson-Saba, J. L. 1983, Ph.D. thesis, Univ. Maryland
- Rothschild, R., et al. 1979, *Space Sci. Instr.*, 4, 265
- Shapiro, S. L., Lightman, A. P., & Eardley, D. M. 1976, *ApJ*, 204, 187
- Shull, J. M., & Van Steenburg, M. 1982, *ApJS*, 48, 95
- Sunyaev, R. A., & Titarchuk, L. G. 1980, *A&A*, 86, 121
- Tanaka, Y. 1992, in *Iron Line Diagnostics in X-Ray Sources*, ed. A. Treves (Berlin: Springer), in press
- Treves, A., et al. 1980, *ApJ*, 242, 1114
- Turner, T. J., & Pounds, K. A. 1989, *MNRAS*, 240, 833
- Turner, T. J., Weaver, K. A., Mushotzky, R. F., Holt, S. S., & Madejski, G. M. 1992, *ApJ*, in press
- White, N. E. 1985, *EXOSAT Express*, 11, 51
- White, N. E., Fabian, A. C., & Mushotzky, R. F. 1984, *A&A*, 133, L9
- White, T. R., Lightman, A. P., & Zdziarski, A. A. 1988, *ApJ*, 331, 939